Proceedings of ASME Turbo Expo 2011
GT2011
June 6-10, 2011, Vancouver, British Columbia, Canada

GT2011-46556

METHOD AND MEASUREMENT OF ADIABATIC WALL TEMPERATURE DOWNSTREAM OF A HIGH PRESSURE TURBINE USING THIN-FILM SENSORS

V. Pinilla, J.P. Solano, G. Paniagua
von Karman Institute for Fluid Dynamics
Turbomachinery & Propulsion Department
Chaussée de Waterloo, 72
1640 Rhode Saint Genèse, Belgium

ABSTRACT

During engine development, heat loads in the turbomachinery are analyzed based on theoretical and numerical estimates together with correlations. Accurate models of the convective fluxes are vital to assess the thermo-mechanical integrity. This paper reports an experimental heat transfer research in a 1.5 turbine stage, the researched model is a the structural vane of a multi-splittered low pressure vane located downstream of a high pressure turbine stage. This concept is envisioned for ultra-high bypass-ratio aero-engines with a swan-neck diffuser between the high-pressure turbine and the low-pressure turbine. Measurements were performed in the large compression tube facility of the von Karman Institute, at representative conditions of modern aero-engines. Double-layered thin film gauges were employed for the measurement of the time-dependent temperature distribution around the airfoil. The initial temperature of the structural vane was adjusted using a heating system. The experimental procedure has allowed the determination of the time-mean and unsteady adiabatic wall temperature. Hence this technique allows the determination of the non-dimensional Nusselt number and proper scaling of the surface temperature to engine conditions. Furthermore, the analysis of the unsteady data reveals the contribution of the temperature fluctuations to the unsteady heat fluxes.

INTRODUCTION

The thermal design, evaluation and management of turbomachinery components require invariant descriptors of the heat transfer process. Moffat [1] proposed the use of Green's functions and the adiabatic heat transfer coefficient, $h_{adiabatic}=q/(T_{adiabatic}-T_{wall})$, for the characterization of the forced convection. Based on the early work of Sellars [2], Anderson and Moffat [3] developed the temperature rise across a passage delimited by two flat plates. In contrast to the use of a mean heat transfer coefficient, $h_{adiabatic}$ is an exclusive function of the fluid mechanics, independent of the thermal boundary conditions. The use of the total temperature upstream of the cascade (instead of the adiabatic value) as driving temperature of the heat flux makes impossible distinguishing the effects of unsteady temperature from changes in the boundary layer, because this temperature is the same all along the airfoil profile.

At Virginia Tech., Popp et al. [4] performed heat transfer measurements in a 2D linear cascade, in particular on the suction side of a transonic passage. The adiabatic wall temperature was obtained by plotting the experimental wall temperature in function of the heat flux. The wall temperature extrapolated at zero heat flux rate corresponds to the adiabatic value. The wide wall temperature variations, during the long testing run (about 25 s.), allowed to perform a linear fit of the raw heat flux with high accuracy. The same approach was recently utilized by Polanka et al., 2008 [5].

At Oxford University, Thorpe et al. [6], [7], and [8] investigated the time-mean and time-resolved heat transfer on the casing wall of an axial turbine, operating at engine representative flow conditions. The adiabatic flow temperature is obtained by performing multiple short tests (less than 1 s.) modifying the substrate temperature with Peltier heat pumps. This methodology yields a distribution of heat flux at different wall temperatures, subsequently a straight line is fitted to calculate the wall temperature, that results in zero heat flux, namely the adiabatic level.

The present research is focused on the steady and unsteady heat transfer, adiabatic wall temperature, and convective heat transfer coefficient measurements in a multisplittered low-pressure vane, downstream of a high pressure turbine rotor. In particular, the test specimen is the structural vane of the multisplitter cascade. The results allow the detailed study of heat fluxes, detaching the influence of the

variation in fluid flow, from the changes in boundary layer status. To the authors' knowledge this is the first time in the open literature that unsteady adiabatic wall temperatures on 3D vanes are documented at engine representative conditions.

Nomenclature

C airfoil chord [m]
C_p specific heat at constant pressure [J kg^{-1} K^{-1}]
D diameter of the nozzle [m]
F frequency [kHz]
g pitch [m]
H airfoil height [m]
h convective heat transfer coefficient [W m^{-2} K^{-1}]
k thermal conductivity [W m^{-1} K^{-1}]
N rotational speed [RPM]
P pressure [bar]
q heat flux [W m^{-2}]
S airfoil abcissa [m]
T temperature [K]
t time [s]
U peripheral speed [m s^{-1}]
v absolute velocity [m s^{-1}]
x axis perpendicular to the gauges surface [m]

Dimensionless groups

Nu Nusselt number, hC/k
Re Reynolds number, ρvC/μ

Greek symbols

α thermal diffusivity [m^2 s^{-1}]
μ kinematic viscosity [m^2/s]
ρ density [kg/m^3]
ψ phase [-]

Subscripts

0 Free-stream or total conditions
1 Stator inlet
2 Stator-rotor interface
3 Rotor outlet
4 low pressure vane outlet
i initial
w wall
ad adiabatic

Superscripts

¯ Time-averaged value
' Unsteady value

EXPERIMENTAL APPARATUS

1.5 turbine model

Measurements were performed on one and a half turbine stage. The upstream high-pressure stage consists of 43 vanes and 64 blades. The low-pressure vane is displayed in Figure 1-a where three small aerodynamic airfoils are located between structural vanes, in total 16 structural vanes are fit within 48 aero vanes.

Turbine rig

Figure 1-b displays the test section, located between a piston pressurized cylinder, and the downstream dump tank at low pressure. Typically the piston compresses the cylinder volume to 2.3 bar and 480 K. A variable sonic throat is used to adjust the downstream turbine pressure. By means of a vacuum system the pressure level in the test section and dump tank is set equal to about 30 mbar. The rotor is then spun-up to almost its design speed from 0 RPM to 6790 RPM in around 7 min. After the pre-test rotation, air in the tube is compressed by the piston, and released into the test section through a fast opening shutter.

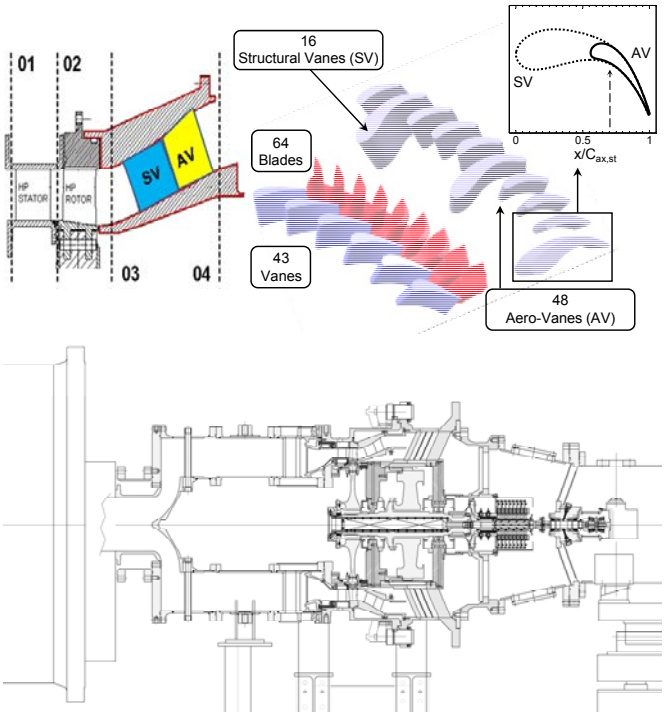

Figure 1. a) High-pressure turbine and multi-splittered low-pressure turbine configuration. b)Turbine test rig

Airfoil heating system

The experimental determination of the adiabatic wall parameters required the heating of the airfoil surface at different temperatures prior to the test. A set of electrical resistors were connected in series and deposited on the structural vane hub and tip, as shown in Figure 2. The electrical assembly was connected to an adjustable power supply, providing a maximum power of 10W. The resistors were glued to the metallic surface with a high thermal conductivity paste, and were isolated from the casing of the turbine with a double strip plastic adhesive. This maximized the amount of heat

generated in the resistors flowing towards the core of the airfoil.

In order to assess the heating methodology, a numerical simulation of the heat conduction phenomenon was carried out, using the commercial software Fluent. A three-dimensional model of the metallic structural vane was meshed, including the casing supports. The presence of the polyamide layer was accounted for using the shell-conduction model. Uniform heat flux q=300 W/m^2 was imposed as boundary condition on the hub and tip of the airfoils. A convective heat transfer coefficient h=3 W/m^{2}K was prescribed between the airfoil sides and the ambient ($T_\infty = 298K$), as the heating takes place with still air.

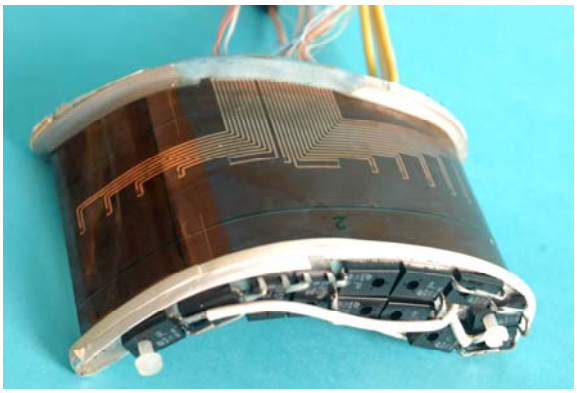

Figure 2. Heaters on the hub of the structural vane

The outside temperature distribution around the airfoil is presented in Figure 3 for the given boundary conditions. Maximum differences of 1K were obtained along the structural vane surface, proving that the procedure of heating the vane from the hub and tip retrieved a fairly uniform temperature distribution, compensating the losses to the ambient and casing. Similarly, the maximum power dissipated by the resistors provided temperatures as high as 400 K.

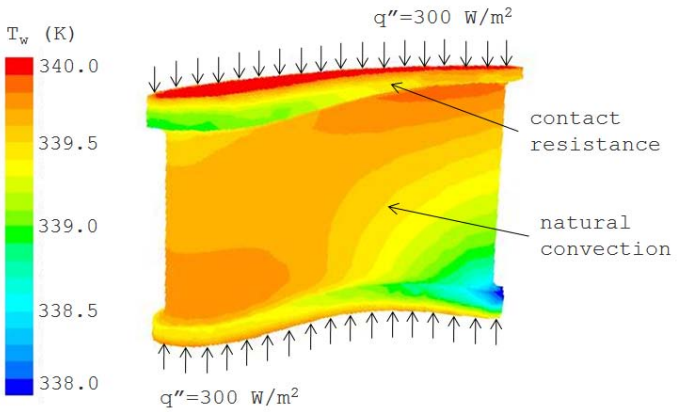

Figure 3. Numerical assessment of the initial temperature distribution under uniform heating.

Surface temperature measurement technique

Double-layered thin film gauges are employed for the measurement of the time-dependent temperature distribution around the airfoil midspan. The thin film temperature gauges consist of a 2.5 mm serpentine nickel thin-film with a resistance of 60 Ω deposited on an Upilex-S polyamide sheet, produced by TAO Systems (see Figure 4). This instrumented plastic thin layer is glued on the blade surface with a double-sided adhesive sheet. The sensing element of the thin-film acts as a variable resistance thermometer, whose resistance variation is monitored by a Wheatstone bridge. The use of copper paths allows performing connections with a negligible resistance. Due to the resulting thickness of the thin-film gauge and its high thermal conductivity, the frequency response of the sensor can be as high as 50 kHz. 28 gauges were deposited on the cross-sectional area of the airfoil (see Figure 2). In order to be able to measure surface temperature changes at the time scale of the test duration (0.5 s) and the rotor blade passing events, an analogue filter was implemented with a gain increasing in frequency. In order to retrieve the temperature fluctuations, a demodulation routine [9] was implemented in Matlab.

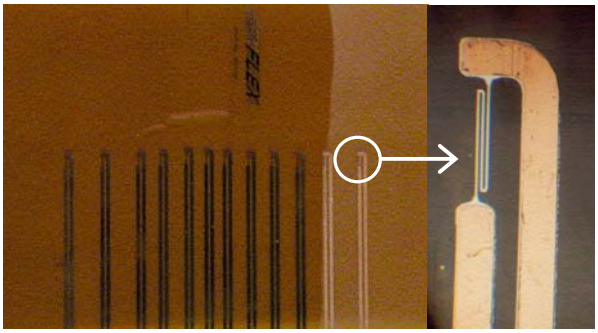

Figure 4. Double-layered thin film gauge.

ADIABATIC WALL TEMPERATURE EVALUATION

Experimental methodology

Five comprehensive tests have been performed in the CT3 rotating cascade, with initial temperatures of the structural vane ranging from ambient conditions (cold test) to $T_{w,i}$= 400 K (pre-heated tests). Figure 5 depicts the temperature evolution for a single gauge during the testing sequence for the five different tests. The substrate is sequentially heated with an adjustable power supply. During the pre-test rotation, windage and ventilation occur, yielding to a progressive wall temperature increase for the cold test. A discussion of the mechanisms involved in this flow-induced pre-heating is found in Solano and Paniagua [10]. For the four remaining tests, the pre-heated temperature decreases during the spinning up period, owing to convection towards the air contained in the test section. At the end of the pre-test rotation, the cross-sectional area of the vane at midspan presents a non-uniform temperature distribution, with a corresponding wall heat flux profile. The appropriate measurement of the unsteady heat transfer during the blow

down test requires the determination of the initial condition, i.e. the temperature distribution when the short-duration test starts (t_s). Then, the unsteady heat conduction equation Eq. (1) must be solved initially in the cross-sectional area of the airfoil for the pre-test rotation, using the time-step of the sampling frequency Δt=1 s. Subsequently, the solution of Eq. (1) for the blow-down (time-step Δt=0.67 ms) provides the transient solution of the heat transfer, which allows deriving the time-mean wall heat flux.

$$\frac{1}{\alpha}\frac{\partial T}{\partial t}=\frac{\partial^2 T}{\partial x^2}+\frac{\partial^2 T}{\partial y^2} \qquad (1)$$

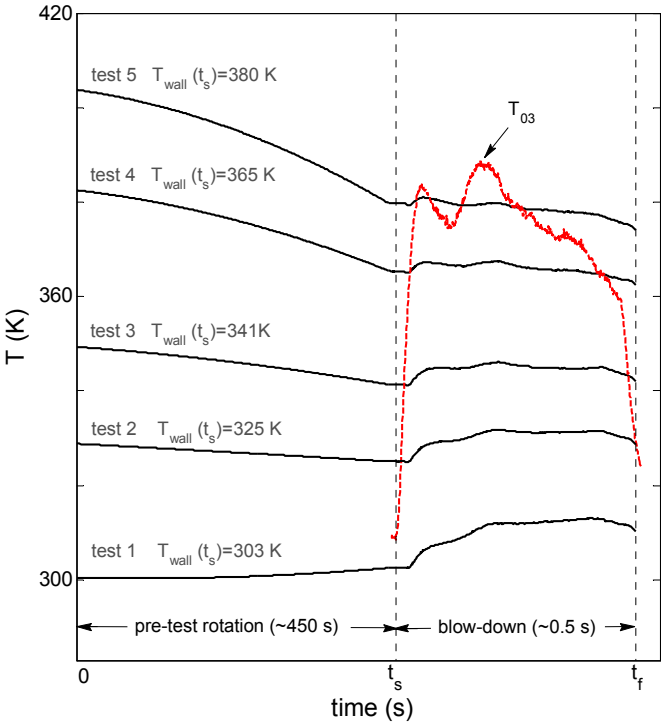

Figure 5. Temperature evolution during the testing sequence for 5 different substrate initial temperatures

Evaluation of the heat flux

Several approaches have been employed for thin film gauge data processing, consisting on analog-circuits (Doorly and Oldfield [11,12]), FFT techniques (Oldfield [13]), or the numerical solution of the unsteady heat conduction equation in the gauge substrate (Iliopoulou et al. [14]). Nevertheless, these methods rely on two assumptions: the substrate can be considered as semi-infinite during the short-duration test, and 1D heat conduction phenomena take place. To account for radial conduction effects actually present at the leading edge of the airfoil (Buttsworth and Jones [15]) and for the failure of the semi-infinite assumption in the trailing edge, the global approach developed by Solano and Paniagua [10] will be considered in this investigation. This data reduction technique consists of solving the 2D unsteady heat conduction equation in the cross sectional area of the vane, using as boundary condition the reconstructed temperature history provided by the thin film gauges in the contour of the airfoil.

A weighted residual (Galerkin) approach is used to derive the finite element equations from the governing differential equation Eq. (1), as stated by Rao [16]. The solution of the resulting algebraic system provides the time-dependent temperature distribution inside the body, and subsequently the normal heat flux to its external boundary, as formulated by Eq. (2).

$$q(x,y,t)=-k_{upilex}\cdot\vec{n}\nabla T \quad x,y\in\partial\Omega \qquad (2)$$

Determination of the time-mean adiabatic wall temperature

In the experiments reported in this work, the determination of the adiabatic wall temperature relies upon the measurement of the time-mean wall heat flux at a range of airfoil wall temperatures. The data produced in the five tests can be plotted as presented in Fig. 6. This figure shows the variation in heat flux as a function of wall temperature for a typical thin film sensor. The straight line that fits the experimental data is also depicted. From the straight line fit, both the mean convective heat transfer coefficient and adiabatic wall temperature can be extracted. The adiabatic wall temperature corresponds to null heat flux, whereas the heat transfer coefficient is established from the slope of the linear correlation.

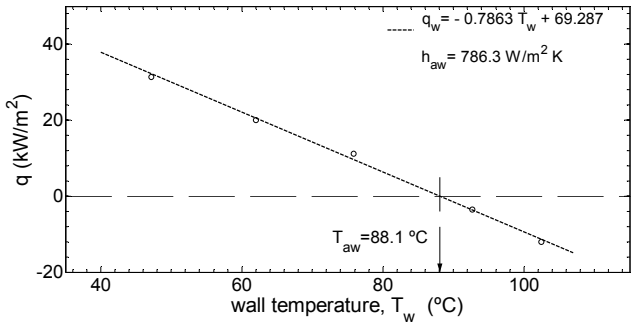

Figure 6. Variation of wall heat flux with airfoil surface temperature. Determination of adiabatic wall temperature.

Unsteady adiabatic wall temperature

The heat flux, adiabatic wall temperature and convective heat transfer coefficient can be decomposed into a time-mean component (corresponding to the procedure displayed in Fig. 6) and an unsteady part. The unsteady component is divided into deterministic and random. The blade passing events modulates the former; hence the dominant frequency of the feat flux is 7.2 kHz. The random unsteadiness is due to turbulence. To obtain the time-resolved signal, the phase locked average is performed. This data reduction tool consists in averaging the heat flux evolution throughout the blade passing periods in order to remove the random unsteady signal. The algorithm has utilized data from fifteen complete revolutions of the rotor, i.e.

960 blade passing events, to derive the mean fluctuation per blade. In this signal, phase (ψ) equals zero when the rotor center of gravity is aligned with the vane leading edge.

The methodology to derive the unsteady adiabatic wall temperature is similar to the steady procedure. For each phase, the unsteady wall temperature is added to the steady wall temperature, and the heat flux as well. Fig. 7 displays the heat flux surface obtained from one gauge as the rotor changes position, at 5 substrate temperatures. A linear regression is obtained for each phase for the 5 wall temperatures. The intersection with the 0 flux plane provides the time-resolved adiabatic wall temperature in function of the rotor position.

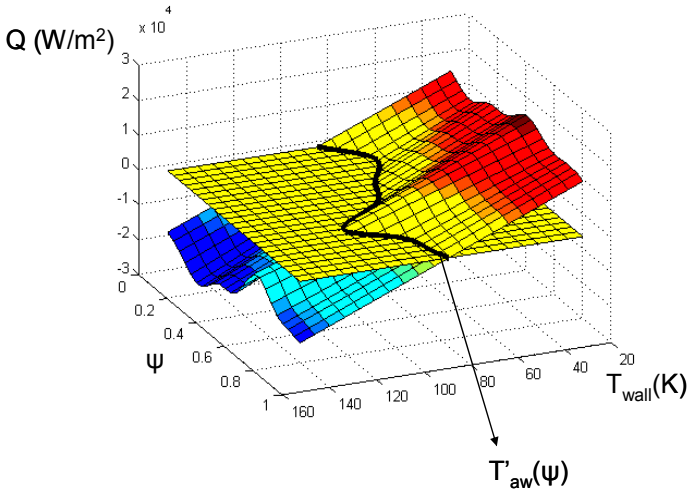

Figure 7. Unsteady adiabatic wall temperature derivation methodology.

RESULTS AND DISCUSSIONS

Time-mean results

Fig. 8 presents the wall heat flux distribution obtained with the Upilex substrate initially at ambient temperature (cold test). The post-processed results are confronted against data obtained with single-layered thin film gauges deposited on a Macor substrate (Pinilla et al [17]). The patterns obtained with both sensor techniques are similar in the leading edge and suction side. However, some different trends are found between both distributions. Probably due to the fact that the figure combines results from several tests performed at slightly different upstream gas temperature.

In order to avoid any dependence from the upstream gas temperature, the adiabatic wall temperature is presented in Fig. 9. Maximum values of adiabatic wall temperature are found in the suction side of the airfoil.

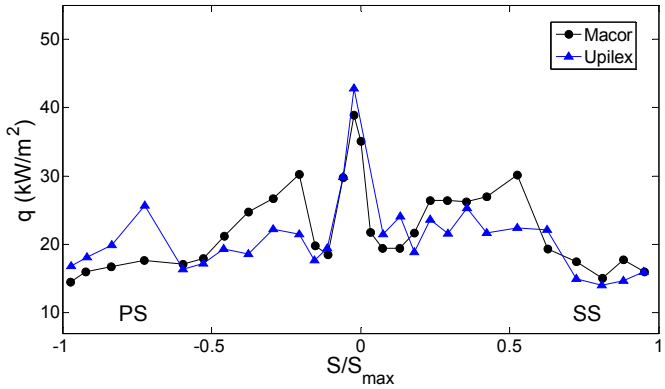

Figure 8. Wall heat flux distributions obtained with single-layered and double-layered thin film gauges

Based on the adiabatic wall temperature the Nusselt number distribution is computed $Nu = \frac{q}{T_{aw} - T_w}\frac{C}{k}$, and depicted in Figure 10. Maximum values of the order of Nu ≈ 4800 are found in the leading edge, with a steep decrease in the front side of the pressure and suction side. Three regions can be identified. In the front part, a steep acceleration occurs for both suction and pressure side, promoted by the large curvature of the structural vane leading edge and the positive flow incidence. Hence, the Nusselt decays abruptly as the laminar boundary layer develops. A sudden increase in the pressure side for S/S_{max}≈-0.2 indicates transition onset with further turbulent boundary layer development. The transition onset in the suction side is found at about S/S_{max}≈0.15. In the rear part, flow is well guided, the turning imposed by the airfoils is enough to oppose the diffusion generated by the high-pressure / low-pressure diffuser.

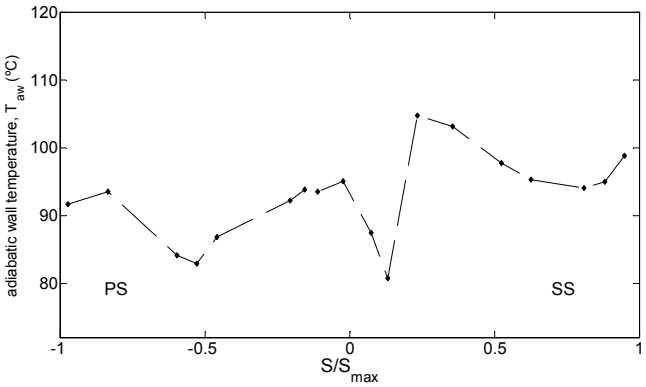

Figure 9. Adiabatic wall temperature distribution in the structural vane at midspan

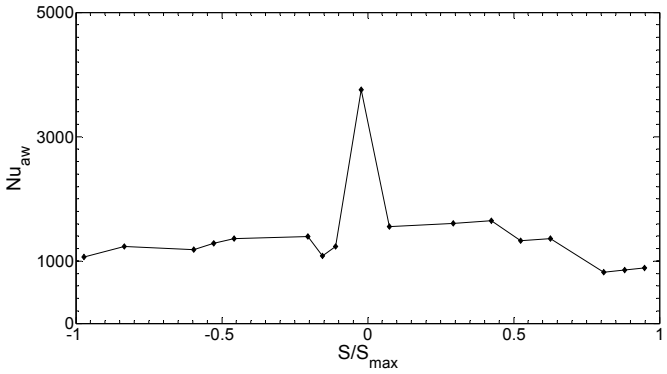

Figure 10. Adiabatic Nusselt number distribution in the structural vane at midspan

Time-resolved results

Fig. 11 exhibits the non-dimensional unsteady heat flux evolution in function of the rotor position (ψ from 0 to 1) in various relevant gauges.

The heat flux variation can be due to the variation in fluid temperature, or to the change in boundary layer status which implies variation of convective heat transfer coefficient. The use of adiabatic wall temperature permits the identification of the driving effects in the unsteady flux fluctuation. Let us decompose the actual heat flux into a steady and unsteady component as set by Eq. 3 and subsequently Eq. 4.

$$\bar{q} + q' = \left(\bar{h}_{aw} + h'_{aw}\right) \cdot \left(\bar{T}_{aw} + T'_{aw} - T_{wall}\right) \quad (3)$$

$$q' = \bar{h}_{aw} \cdot T'_{aw} + h'_{aw} \cdot \bar{T}_{aw} - h'_{aw} \cdot T_{wall} \quad (4)$$

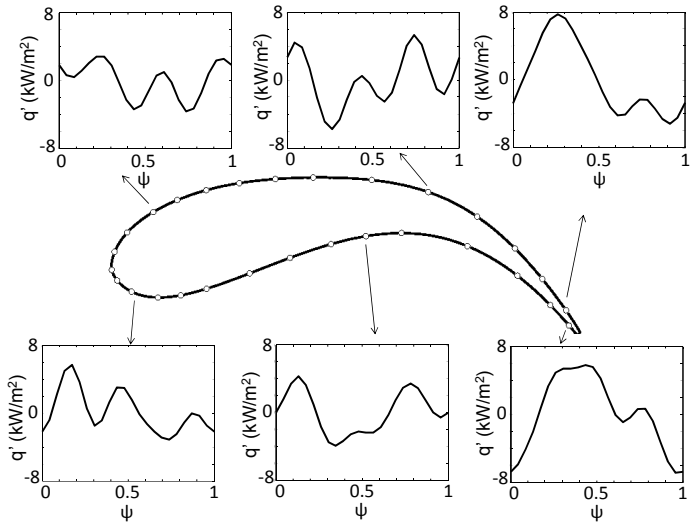

Figure 11. Unsteady heat flux evolution for six representative sensors along the structural vane midspan

In Eq. 4 the term $h'_{aw} \cdot T'_{aw}$ has been neglected because its influence on the unsteady heat transfer is almost zero.

Using this methodology Figure 12 shows the different contributions to the unsteady heat flux. The influence of the unsteady adiabatic wall temperature and unsteady convective heat transfer coefficient on the unsteady heat flux is revealed. The main terms come from the variation of adiabatic wall temperature. By contrast, the variations of convective heat transfer coefficient have a lower influence on the heat transfer. In agreement with common assumptions, the variations on heat transfer are mainly generated by external variations on temperature. The table below shows that the principal influence comes from $\bar{h}_{aw} \cdot T'_{aw}$ and $h'_{aw} \cdot \left(\bar{T}_{aw} - T_{wall}\right)$.

	Influence on q'
$\bar{h}_{aw} \cdot T'_{aw}$	86%
$h'_{aw} \cdot \left(\bar{T}_{aw} - T_{wall}\right)$	14%

The averaging of Eq. 3 unveils a contribution of the unsteady terms into the steady heat flux in unsteady flows.

$$\bar{q} = \bar{h}_{aw} \cdot \left(\bar{T}_{aw} - T_{wall}\right) + \overline{h'_{aw} \cdot T'_{aw}} \quad (5)$$

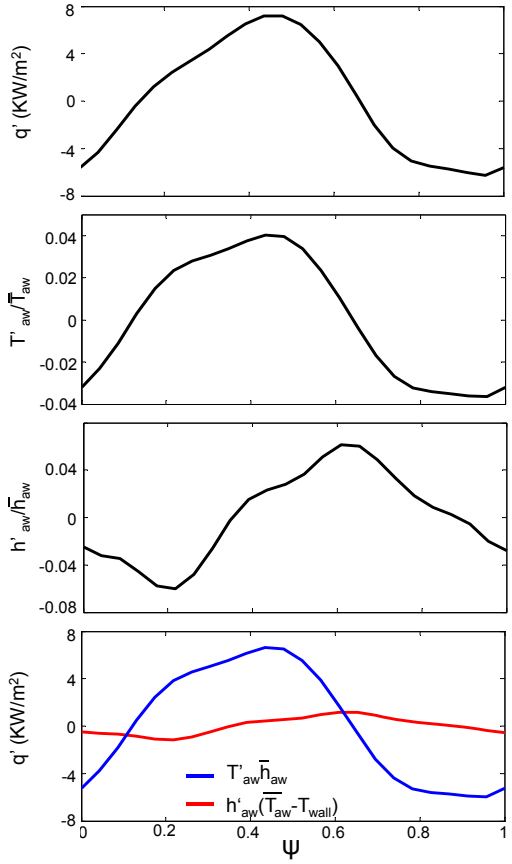

Figure 12. Unsteady heat flux, adiabatic wall temperature, heat transfer coefficient and components q'

The unsteady influence on the mean heat flux varies between 1.1% (at S/S_{max}=0.1) and 8.0% (at S/S_{max}=0.5) of the time-averaged.

CONCLUSIONS

A comprehensive experimental methodology has been developed for the measurement of the adiabatic wall temperature in a 3D vane at engine representative conditions. A heating system allows performing subsequent blow-down tests in a rotating cascade for different airfoil temperatures. The phenomenological relation between the steady-state wall heat flux and the wall temperature retrieves the adiabatic heat transfer coefficient and the adiabatic wall temperature.

Distributions of adiabatic wall temperature and Nusselt number at midspan have been obtained, providing an invariant description of the convective heat transfer phenomena to the airfoil surface.

Time-resolved results on adiabatic heat transfer coefficient have been also obtained. The variation of heat flux due to fluid temperature and variation of boundary layer have been quantified. Experimental results prove that the main contribution to changes in wall heat flux come from the variations in adiabatic wall temperature; meanwhile the variations of convective heat transfer coefficient have a lower influence on the heat transfer. This novel results confirm typical assumptions on some research works, which assume that the turbine boundary layers keep constant and the variations on heat transfer come from external variations on temperature. Furthermore the contribution of unsteadiness to the steady heat flux is of the order of 1 to 8% of the mean level.

ACKNOWLEDGMENTS

The authors would like to thank Tolga Yasa and Sergio Lavagnoli for their valuable assistance in the test campaign. We gratefully acknowledge the financial support of the European Commission and industrial manufacturers that participate in the Project Turbine Aero-Thermal External Flows 2, coordinated by Snecma.

REFERENCES

[1] R.J. Moffat, 1998, “What’s new in convective heat transfer?”. International Journal of Heat and Fluid Flow, (19)2, pp. 90-101.

[2] R.J. Sellars, M. Tribusm, J.S. Kline, 1956, "Heat transfer to laminar flow in a round tube or flat conduit. the Graetz problem extended", Trans. ASME 78, pp. 441-448.

[3] Anderson, A.M., and Moffat, R.J., 1992, "The adiabatic heat transfer coefficient and the superposition Kernel function: part 1 - Data for arrays of flat packs for different flow conditions", Journal of Electronics Packaging, (114), pp. 14-22.

[4] Popp, O., Smith, D.E., Bubb, J.V., Grabowski III, H.C., Diller, T.E., Schetz, J.A., Ng, T.E., 2000, “Investigation of heat transfer in a film cooled transonic turbine cascade, Part I: Steady heat transfer” ASME Paper No. 2000-GT-202.

[5] Polanka, M.D., Anthony, R.J., Bogard, D.G., Reeder, M.F., 2008, "Determination of cooling parameters for a high speed, true scale, metallic turbine vane ring", ASME Paper No. GT-2008-50281.

[6] Thorpe, S.J., Yoshino, S., Ainsworth, R.W., Harvey, N.W., 2004, "An investigation of the heat transfer and static pressure on the over-tip casing wall of an axial turbine operating at engine representative flow conditions (I). Time mean results", International Journal of Heat and Fluid Flow (25)6, pp.933-944.

[7] Thorpe, S.J., Yoshino, S., Ainsworth, R.W., Harvey, N.W., 2004, "An investigation of the heat transfer and static pressure on the over-tip casing wall of an axial turbine operating at engine representative flow conditions (II). Time resolved results", International Journal of Heat and Fluid Flow (25)6, pp.945-960.

[8] Thorpe, S.J., Ainsworth, R.W., 2006, "The effects of blade passing on the heat transfer coefficient of the over-tip casing in a transonic turbine stage", ASME Paper No. GT2006-90534.

[9] Schultz, D.L., Jones, T.V., 1973, "Heat transfer measurements in short duration facilities", AGARD Report, No 165.

[10] Solano, J.P., Paniagua, G., 2009, "Novel 2D transient heat conduction calculation in a cooled rotor: ventilation preheating - blowdown flux", ASME Journal of Heat Transfer, (131), pp. 81601-1-9.

[11] Doorly, J.E., Oldfield, M.L.G., 1986, "New heat transfer gauges for use on multilayered substrates", Journal of Turbomachinery, 108, pp 153-160.

[12] Doorly, J. E., and Oldfield, M. L. G., 1987, “The theory of advanced multi-layer thin film heat transfer gauges,” International Journal of Heat and Mass Transfer, 30(6), pp 1159-1168.

[13 Oldfield, M.L.G., 2006, “Impulse response processing of heat transfer gauge signals”, ASME Paper No. GT-2006-90949.

[14] Iliopoulou, V., Dénos, R., Billiard, N., Arts, T. 2004, “Time-averaged and time-resolved heat flux measurements on a turbine stator blade using two-layered thin-film gauges”, ASME Journal of Turbomachinery, (126), pp. 570-577.

[15] Buttsworth, D. R., and Jones, T. V., 1997, “Radial conduction effects in transient heat transfer experiments”, The Aeronautical Journal, (101)1005, pp. 209-212.

[16] Rao, S.S., 1989, “The Finite Element Method in Engineering”, 2nd Ed, Pergamon Press

[17] Pinilla, V., Solano, J.P., Paniagua, G., Lavagnoli, S., Yasa, T., 2010, “Experimental heat transfer investigation in a multisplitter LP vane Arquitecture”, ASME Paper No. GT2010-22694.

[18] Bronstein, I.N., Semendjajew, K.A., Musiol, G., Mühlig, H., 2008, "Taschenbuch der Mathematik", Verlag Harri Deutsch, Frankfurt am Main.

ANNEX A

UNCERTAINTY ANALYSIS

The uncertainty analysis is based on the guidelines given by Bronstein et al. [18]. All estimates of uncertainty are given at 95% of confidence limit.

In transient heat transfer experiments employing thin-film resistance gauges, the heat transfer rate is determined from the temperature history of the wall surface and temperature is obtained using a resistor gauge. The next analysis is an example of deriving the adiabatic wall temperature uncertainty for a case of T_{aw}=373 K.

Temperature uncertainty

This temperature is calculated as follows:

$$T=f(a, b, a_r, V_i, V_r) = a + b \cdot V_i + a_r \cdot V_r$$

Where the two first terms are the initial temperature and the last term is the variation in temperature during the test. The next table summarized the uncertainty coming from these terms:

Quantity	Mean value	Uncertainty	T uncertainty (%)
a	623	103	1.3
b	-366	7.8	1.1
V_i	0.818	0.004	0.6
a_r	9.35	0.2	0.2
V_r	1.1	0.1	1.1

Heat flux uncertainty

The heat flux is derived solving the thermal equation inside the vane. The uncertainty comes from the thermal properties of the substrate and from the temperature. The next table shows the influence of these parameters:

Quantity	Mean value	Uncertainty	q uncertainty (%)
a	623	10.3	0.2
b	-366	7.8	0.3
V_i	0.818	0.004	0.3
a_r	9.35	0.2	1.8
V_r	1.1	0.1	0.3
$\sqrt{\rho \cdot c \cdot k}_1$	478396	23919	3.8
$\sqrt{\rho \cdot c \cdot k}_2$	65412000	3270600	0.4

Adiabatic wall temperature uncertainty

The adiabatic wall temperature is derived directly from a lineal fitting of a set of points defined by a wall temperature and a heat flux ($T_{aw} = f(T,q)$). So this temperature uncertainty is direct function of the heat flux and wall temperature uncertainties:

Quantity	Uncertainty	T_{aw} uncertainty %
T(K)	14	3.6
q(W/m^2)	120	0.4

This process yields this final adiabatic wall temperature uncertainty: ΔT_{aw}=14 K.